UC Riverside

UC Riverside Previously Published Works

Title

The Swiss army knife of time series data mining: ten useful things you can do with the matrix profile and ten lines of code

Permalink

https://escholarship.org/uc/item/6rw5v40f

Journal

Data Mining and Knowledge Discovery, 34(4)

ISSN

1384-5810

Authors

Zhu, Yan
Gharghabi, Shaghayegh
Silva, Diego Furtado
et al.

Publication Date

2020-07-01

DOI

10.1007/s10618-019-00668-6

Peer reviewed

The Swiss army knife of time series data mining: ten useful things you can do with the matrix profile and ten lines of code

Yan Zhu[1] · Shaghayegh Gharghabi[1] · Diego Furtado Silva[2] · Hoang Anh Dau[1] ·
Chin-Chia Michael Yeh[1] · Nader Shakibay Senobari[1] · Abdulaziz Almaslukh[1] ·
Kaveh Kamgar[1] · Zachary Zimmerman[1] · Gareth Funning[1] · Abdullah Mueen[3] ·
Eamonn Keogh[1]

Abstract

The recently introduced data structure, the Matrix Profile, annotates a time series by recording the location of and distance to the nearest neighbor of every subsequence. This information trivially provides answers to queries for both *time series motifs* and *time series discords*, perhaps two of the most frequently used primitives in time series data mining. One attractive feature of the Matrix Profile is that it completely divorces the high-level details of the analytics performed, from the computational "heavy lifting." The Matrix Profile can be computed using the appropriate computational paradigm for the task at hand: CPU, GPU, FPGA, distributed computing, anytime computation, incremental computation, and so forth. However, all the details of such computation can be hidden from the analyst who only needs to think about her analytical need. In this work, we expand on this philosophy and ask the following question: If we assume that we get the Matrix Profile for free, what interesting analytics can we do, writing at most ten lines of code? As we will show, the answer is surprisingly large and diverse. Our aim here is not to establish or compete with state-of-the-art results, but merely to show that we can both reproduce the results of many existing algorithms and find novel regularities in time series data collections with very little effort.

✉ Yan Zhu
  yzhu015@ucr.edu

  Eamonn Keogh
  eamonn@cs.ucr.edu

[1] University of California, Riverside, Riverside, USA

[2] Federal University of São Carlos, São Carlos, Brazil

[3] University of New Mexico, Albuquerque, USA

 🍀 Springer

1 Introduction

The recently introduced time series data structure, the Matrix Profile, annotates a time series by recording the location of and distance to the nearest neighbor of every subsequence (Yeh et al. 2016b; Zhu et al. 2016). This means that it encodes all the information needed to answer both *time series motif* and *time series discord* queries, perhaps two of the most frequently used primitives in time series data mining (Li et al. 2015; Mueen et al. 2009; Yankov et al. 2007; Yeh et al. 2016b; Zhu et al. 2016). Both of these primitives can be discovered in other ways; however, the Matrix Profile can be computed very efficiently, regardless of the length of the subsequences considered (i.e., the dimensionality). This is a useful property because all other algorithms that compute these primitives suffer greatly from the curse of dimensionality (Li et al. 2015; Mueen et al. 2009; Yankov et al. 2007). For example, before the invention of the Matrix Profile, no one attempted to discover motifs longer than 900 datapoints long (Li et al. 2015; Mueen et al. 2009; Yankov et al. 2007). In contrast, Yeh et al. (2016b) demonstrates a successful experiment in bioinformatics that requires finding motifs of length 60,000. Similarly, before the Matrix Profile, the longest dataset searched for *exact* motifs was a million datapoints long (Li et al. 2015; Mueen et al. 2009; Yankov et al. 2007), but Zhu et al. (2016) increases that record one-hundred fold.

While the scalability of the Matrix Profile is an attractive and enabling property, it is not its most interesting feature. The original Matrix Profile paper concludes with the sentence, "*There are many avenues for future work, and we suspect that the research community will find many uses for the matrix profile*." (Yeh et al. 2016b). Recently this claim has been borne out in a series of papers to show that the Matrix Profile can be used to support a host of analytic tasks including: semantic segmentation (Gharghabi et al. 2017), the discovery of evolving patterns (time series chains) (Zhu et al. 2017), and finding predictive patterns in weakly labeled data (Yeh et al. 2017). It is the extraordinary *generality* of the Matrix Profile that is its most important and useful feature. To support this somewhat subjective claim, in this work we make a more concrete claim. Given just the Matrix Profile, and at most ten lines of additional code (in a high-level language, here we use Matlab), one can perform a host of analytic tasks, as well as reproduce the results of much more complicated algorithms.

Philosophically, we would like the community to regard the Matrix Profile much like most programmers regard the `sort` subroutine in their favorite language. A casual programmer does not care or need to know how it is implemented (quick-sort, merge-sort, heap-sort etc.), she regards it as computationally "free[1]," and she uses it

---

[1] We will revisit the idea of computationally "free" for the Matrix Profile in Sect. 4. For the case of sorting numbers, most invocations of sorting are on less than one million numbers, and it is possible to sort a million 32-bit numbers on a modern machine in 20 ms with essentially no space overhead. Thus, for most applications/users, it makes sense to think of sorting as a no-cost resource. Clearly, sorting can be a bottleneck for some applications, but these are rare enough that we think our claim is self-evident.

to solve many problems. In a similar spirit, a data analyst does not need to know how the Matrix Profile is computed (It could be by STAMP (Yeh et al. 2016b), STOMP (Zhu et al. 2016), STOMP*I* (Yeh et al. 2018), SCRIMP++ (Zhu et al. 2018), etc.), she can typically regard it as computationally "free" and use it to solve many time series data mining problems. We regard this simple abstraction as *game changing*. Analysts are much more likely to try out a new idea if they could get the first results in a few minutes, including both coding time and computational time. A tentative idea that take hours or days to produce may never get past the idea stage.

The rest of this paper is organized as follows. After a brief review of the Matrix Profile in Sect. 2, in Sect. 3 we will show ten case studies that support our claim that many interesting problems can be solved using the Matrix Profile and at most ten lines of additional code. In Sect. 4, we will offer conclusions and directions for future work.

2 General related work and background

In the following section we briefly review the notion and definitions necessary to understand the Matrix Profile (Yeh et al. 2016a, b, 2017, 2018; Zhu et al. 2016, 2017, 2018). Readers familiar with this material can skip ahead to Sect. 3.

2.1 Definitions and notation

We begin by defining the data type of interest, *time series*:

Definition 1 A *time series* $T \in \mathbb{R}^n$ is a sequence of real-valued numbers $t_i \in \mathbb{R}$: $T = [t_1, t_2, \ldots, t_n]$ where n is the length of T.

We are not interested in the *global*, but the *local* properties of a time series. A local region of a time series is called a *subsequence*:

Definition 2 A *subsequence* $T_{i,m} \in \mathbb{R}^m$ of time series T is a continuous subset of the values from T of length m starting from position i. Formally, $T_{i,m} = [t_i, t_{i+1}, \ldots, t_{i+m-1}]$, where $1 \leq i \leq n - m + 1$, and m is a user-defined subsequence length.

We can extract all the subsequences from a given time series by sliding a window of size m across the time series. This is called an *all-subsequence set*:

Definition 3 An *all-subsequence set* A of a time series T is an ordered set of all the subsequences of T: $A = \{T_{1,m}, T_{2,m}, \ldots, T_{n-m+1,m}\}$. We use A_i to denote $T_{i,m}$.

Note the all-subsequence set is defined purely for notational purposes. In our implementation, we do not actually *extract* the subsequences in this form as it would require significant time overhead, and explode the memory requirements.
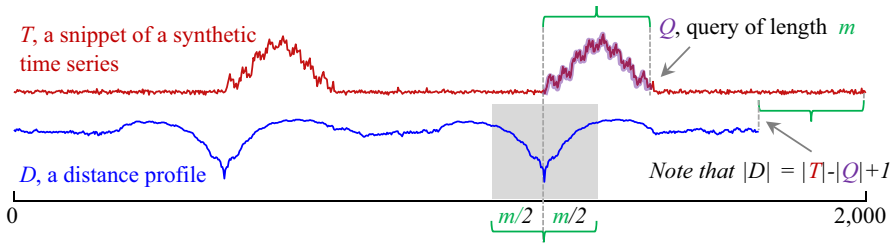
Fig. 1 A subsequence Q extracted from a time series T is used as a query to every subsequence in T. The vector of all distances is a distance profile

We can take any subsequence from a time series and compute its distance to all the sequences in an all-subsequence set. We store these distance values in a vector called the *distance profile*:

Definition 4 A *distance profile D* is a vector of the Euclidean distances between a given query subsequence and every subsequence in the all-subsequence set.

We assume the distance is measured as the Euclidean distance between the z-normalized subsequences (Bayardo et al. 2007).

The first four definitions are illustrated in Fig. 1.

Note the query subsequence and the all-subsequence set may or may not belong to the same time series. By definition, if the query subsequence and the all-subsequence set belong to the same time series, the distance profile must be zero at the location of the query, and close to zero just before and after (assuming only that the time series is somewhat smooth). Such matches are called *trivial matches* in the literature (Mueen et al. 2009), and are avoided by ignoring an exclusion zone (shown as a gray region) of $m/2$ before and after the location of the query. Practically, we set the distance values in the exclusion zone to infinity.

The minimum value of a distance profile indicates the nearest neighbor (i.e., *1NN*) of the given query subsequence within the all-subsequence set. We are interested in finding the nearest neighbor of *every* subsequence; this constitutes a *similarity join set*:

Definition 5 *Similarity join set:* given two all-subsequence sets A and B, a similarity join set J_{AB} of A and B is a set containing pairs of each subsequence in A with its nearest neighbor in B: $J_{AB} = \{\langle A_i, B_j \rangle | \theta_{1nn} (A_i, B_j)\}$. Here $\theta_{1nn} (A_i, B_j)$ is a Boolean function which returns "true" only if B_j is the nearest neighbor of A_i in the set B. We denote the similarity join set formally as $J_{AB} = A \bowtie_{\theta 1nn} B$.

We use two vectors, the *matrix profile* and the *matrix profile index*, to store the nearest neighbor information of a similarity join set. The *matrix profile* stores the distances between all the subsequences and their nearest neighbors:
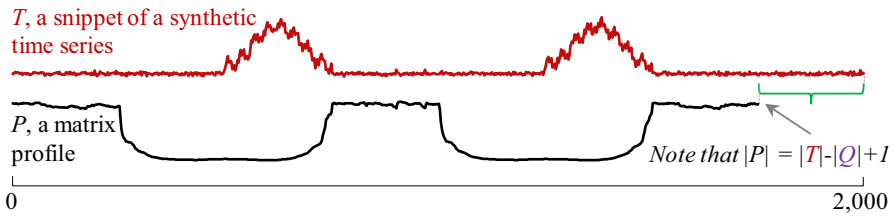
Fig. 2 A time series T, and its self-join matrix profile P

Definition 6 A *matrix profile* P_{AB} is a vector of the Euclidean distances between each pair in J_{AB}, where the ith element of P_{AB} is the distance between A_i and its nearest neighbor in B.

We call this vector a matrix profile since it could be computed by using the full distance matrix of all pairs of subsequences in time series T, and evaluating the minimum value of each row (although this method is naïve and space-inefficient). Figure 2 shows the matrix profile of our running example.

The ith element in the matrix profile P indicates the Euclidean distance from subsequence $T_{i,m}$ to its nearest neighbor in time series T. However, it does not indicate the location of that nearest neighbor. This information is recorded in a companion data structure called the *matrix profile index*:

Definition 7 A *matrix profile index* I_{AB} of a similarity join set J_{AB} is a vector of integers where the ith element of I_{AB} is j if $\{\langle A_i, B_j \rangle\} \in J_{AB.}$

By storing the neighboring information in this manner, we can efficiently retrieve the nearest neighbor of query A_i by accessing the ith element in the matrix profile index.

In general, the function which computes the similarity join set of two input time series is not symmetric: $J_{AB} \neq J_{BA}$, $P_{AB} \neq P_{BA}$, and $I_{AB} \neq I_{BA}$, except in the special case where $A = B$.

We can regard the matrix profile as a *meta* time series annotating the time series T if the matrix profile is generated by joining T with itself (i.e., $A = B$). This profile has a host of interesting and exploitable properties. For example, the highest point on the profile corresponds to the time series discord (Chandola et al. 2009), the (tying) lowest points correspond to the locations of the best time series motif pair (Mueen et al. 2009), and the variance can be seen as a measure of the T's complexity.

We call this special case of similarity join set (Definition 5) a *self-similarity join set*, the corresponding matrix profile a *self-similarity join matrix profile*, and the corresponding matrix profile index a *self-similarity join matrix profile index*.

Definition 8 A *self-similarity join set* J_{AA} is the similarity join of an all-subsequence set A with itself. We denote this formally as $J_{AA} = A \bowtie_{\theta 1nn} A$. We denote the

corresponding self-similarity join matrix profile as P_{AA}, and the corresponding self-similarity join matrix profile index as I_{AA}.

For clarity of presentation, we have confined this work to the single dimensional case; however, nothing about our work intrinsically precludes generalizations to multidimensional data. In the multidimensional data, we would still have a single *matrix profile*, and a single *matrix profile index*; the *only* change needed is to replace the one-dimensional Euclidean Distance with the *b*-dimensional Euclidean Distance, where *b* is the number of dimensions the user wants to consider.

2.2 Summary of the previous section

Since the previous section was rather dense, here we summarize the main takeaway points. We can create two meta time series, the *matrix profile* and the *matrix profile index*, to annotate a time series *A* with the distance *to* and location *of* all its subsequences' nearest neighbors in itself or another time series *B*. These two data objects explicitly contain the answers to the time series data mining tasks of motif discovery and discord discovery (Yeh et al. 2018). Moreover, as we will show below, we can easily perform many other kinds of analytics using the *matrix profile* and the *matrix profile index* as primitives.

To make the contributions of this work more concrete, we will occasionally show the actual code we use to solve various problems. The two basic tools that perform the key operations explained above are:

```
[MP, MPindex] = computeMatrixProfile(T,m);        % Def 8
[JMP, JMPindex] = computeMatrixProfileJoin(A,B,m); % Def 6-7
```

Once again, a key assumption of this work is that these operations can be computed very fast, by any one of half a dozen algorithms optimized for various computational paradigms. Thus we simply take these operations as given, and see what we can do with them with just a tiny amount of extra coding effort.

3 Ten useful things you can do with the matrix profile and ten lines of code

In this section, we show the eponymous *ten useful things you can do with the matrix profile and ten lines of code*. In every case we make the data available (Supporting Webpage 2019). The code to compute the matrix profile can be found at The UCR Matrix Profile Page (2017) and the remaining code is placed inline in this work. Note that we see these as ten *demonstrations*. We do not expand any section with the rigor one might expect if it were a single idea being presented in a paper.
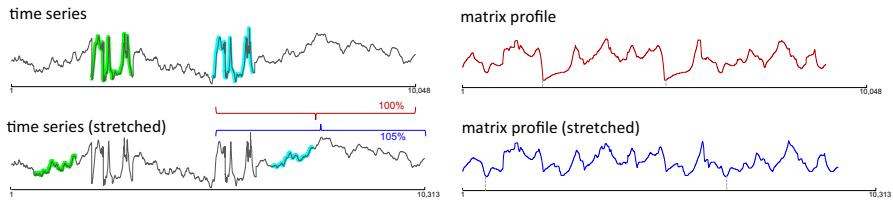
Fig. 3 (Top left) A random walk time series with two exemplars from the MALLAT dataset imbedded at locations 2001 and 5025. The color highlighting indicates the top-1 motif, which unsurprisingly are exactly the imbedded patterns. (Top right) The matrix profile corresponding to the random walk time series. The minimum values correspond to the top-1 motif in the time series. (Bottom left) The same time series, but with the second half linearly stretched by 5%. This causes the top-motif to change to snippets of random walk. (Bottom right) The matrix profile corresponding to the stretched time series. We can see that the minimum points changed (Color figure online)

3.1 Discovering motifs under uniform scaling

The utility for motif discovery under uniform-scaling invariance was first considered in Yankov et al. (2007). We revisit the motivation with a simple and visually compelling example. We took two exemplars from the same class from the MALLAT dataset (Chen et al. 2015) and imbedded them into a random walk dataset. As Fig. 3 top shows, even without the color-coded clue brushed onto the data by the Matrix Profile discovery tool (The UCR Matrix Profile Page 2017), the repeated pattern is visually obvious.

We then took the second half of the time series and linearly stretched it by 5%. By any standard, such a change is a trivial difference and essentially visually imperceptible. Nevertheless, as Fig. 3 bottom shows, the pair of imbedded patterns are no longer the top-1 motif, an unexpected and disquieting result. Before we show how to address this within this paper's "the Matrix Profile plus ten-lines-of-code framework," we note the following facts that mitigate the issue.

- For the rescaled version, the pair of imbedded patterns was the *second*-best motif and only *just* nudged out by the spurious random walk pair.
- If, instead of searching with a motif length of 1024, the original length of the imbedded pattern, we had searched for a shorter length, say 500, then the best motif would have been a subsequence of the imbedded pattern. The user could then have examined the shorter motif and realized it could be extended significantly while maintaining its similarity.
- We deliberately chose this dataset, from the 85 in the UCR archive, knowing it would be very sensitive to changes in linear scaling. This is because *complex* time series (see Batista et al. 2014) with very sharp rises and falls are particularly sensitive to having features out of phase. For most datasets, motif discovery is much more robust to small amounts of uniform scaling.

Despite all these mitigating facts, Fig. 3 bottom clearly shows that there may be some situations in which there is a need to find motifs with invariance to uniform scaling. To
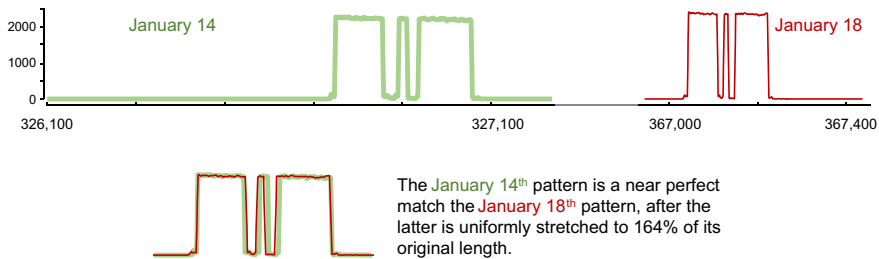
Fig. 4 (Top) Two non-contagious snippets from the ElectriSense dataset (Gupta et al. 2010). While semantically similar, they have a very large Euclidian distance because they are of different lengths. (Bottom) After stretching the January 18th pattern by 164%, the two patterns are almost identical

the best of our knowledge, there is only one research effort that has addressed this. However, this method is *approximate*, requires many parameters to be set, and is only able to support a limited range of scaling (Yankov et al. 2007). In contrast, we can easily and *exactly* solve this problem under our simple assumptions.

For the moment, assume that we know the scaling factor we want to be invariant to happens to be 1.64. We can take the dataset T and copy a stretched version of it into $T2$, simply by using:

```
T2 = T(1: 100/164: end); % Unofficial Matlab way to resample
```

If we now call:

```
[JMP, JMPindex] = computeMatrixProfileJoin(T,T2,500);
```

Now, the resulting Matrix Profile will discover the motifs with the appropriate uniform scaling invariance. In fact, we did exactly this on a 6,106,456 length trace of household electrical demand to discover the motif shown in Fig. 4.

The motif pattern appears to be the three elements of a dishwasher cycle (clean, rinse, dry), which can take different amounts of time due to the use of the optional *half-load* feature (LG Dishwasher Owners Manual 2017). In this case, we knew from some first principle physics how to set the scaling factor, but that may not always be the case. Given our assumptions, we can simply iterate over all possible scaling factors in a given range. For example, to discover motifs that are similar after scaling one pattern by 150–180%, we can use the following code snippet.

```
minJMP=inf(1,length(T)), minScale=ones(1,length(T));
minJMPindex=zeros(1,length(T));
for scale_factor = 150 : 180
  T2 = T(1: 100/scale_factor: end);
  [JMP, JMPindex] = computeMatrixProfileJoin(T,T2,500);
  locs = JMP < minJMP;
  minJMP(locs)=JMP(locs),  minScale(locs)=scale_factor/100;
  minJMPindex(locs)=JMPindex(locs);
end
```

This example perfectly elucidates the philosophy driving this paper. For many time series data mining tasks, we may not need to spend significant human time designing, implementing and tuning new algorithms. The Matrix Profile and ten lines of code may be sufficient.

3.2 Discovering time series semordnilaps

Consider the sentence fragment we discovered in Wikipedia, "… *the longest-lived Tasmanian devil recorded was Coolah…*" (Tasmanian devil 2017). This snippet contains a Semordnilap pair (Puder 2000), the mirrored words "lived" and "devil". Semordnilaps are easy to find in arbitrary text strings, and indeed have an important role in molecular biology. For example, many restriction enzymes recognize specific palindromic sequences and cut them. As a concrete example, the restriction enzyme EcoRI recognizes the following palindromic pair, "GAATTC" and "CTT AAG" (Kurpiewski et al. 2004).

Because the original definition of time series motifs was directly inspired by the analogy to DNA, it is natural to ask if there is a natural time series analogy to semordnilaps, and if so, can they be efficiently discovered? From the previous example, the reader will readily see that this is trivial, we can simply use:

```
T2 = fliplr(T);  % returns T reversed
[JMP, JMPindex] = computeMatrixProfileJoin(T,T2,m);
```

The only question remaining is: are there *natural* domains that contain time series semordnilaps? The answer is affirmative.

To demonstrate the utility of Semordnilap discovery, we consider Joseph Haydn's Symphony No. 47 in G major, written in 1772. In particular, we examined a performance by the Tafelmusik Orchestra, directed by Bruno Weil in 1993 (Music Performance 2017). The performance is 21 min and 2 s long. As shown in Fig. 5 top, we converted it to Mel-frequency cepstral coefficients (MFCC) using windows with
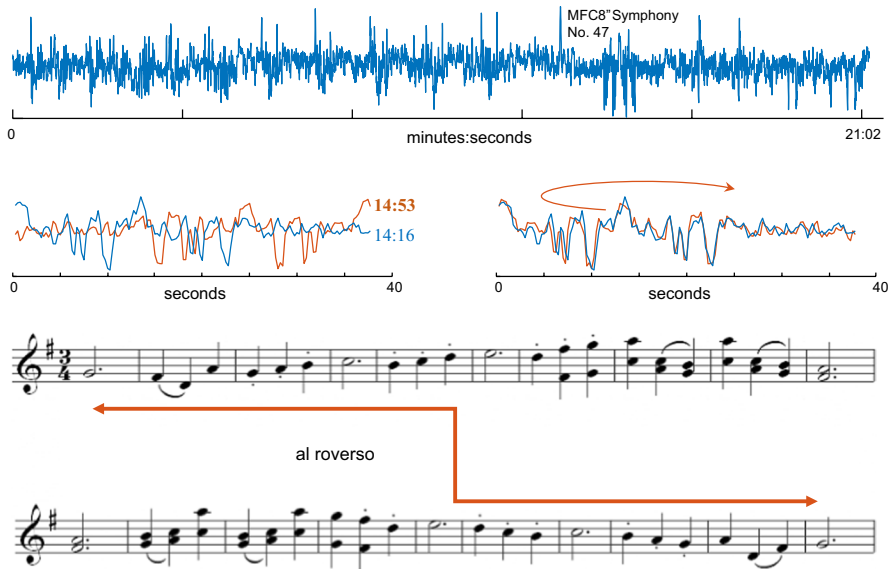
Fig. 5 (Top) Haydn's Symphony No. 47 converted to MFCC. (Center left) Two snippets found by Semordnilap discovery appear unrelated until we flip one backwards in time (center right). (Bottom) The sheet music for the relevant section explains this unexpected discovery

0.5 s and 50% of overlap (standard music processing settings). We set m to 150, or 37.5 s.

At 14 min and 53 s, there is a Semordnilap of a passage we encountered at 14 min and 16 s.

Figure 5 bottom explains the presence of such a perfectly conserved Semordnilap. As noted in Bonds (1998), "*The most extraordinary of all canonic movements from this time is of course from Symphony No. 47. Here Haydn writes out only one reprise of a two-reprise form, and the performer must play the music 'backward' the second time around*".

While this example is clearly contrived, there may be Semordnilaps waiting to be discovered in dance, travel trajectories, medical data, industrial processes, and a host of domains that have yet to occur to us.

3.3 Discovering time series reverse complements

Our success in finding Semordnilaps immediately suggests another specialized type pattern we could search for. Are there examples of patterns which repeat, but in which one pattern is the inverse of the other? That is to say, unlike Semordnilaps, which are "flipped" in the *time* axis, are there patterns that are flipped upside-down in the *value* axis? We call such patterns Time Series Reverse Complements (TSRCs).
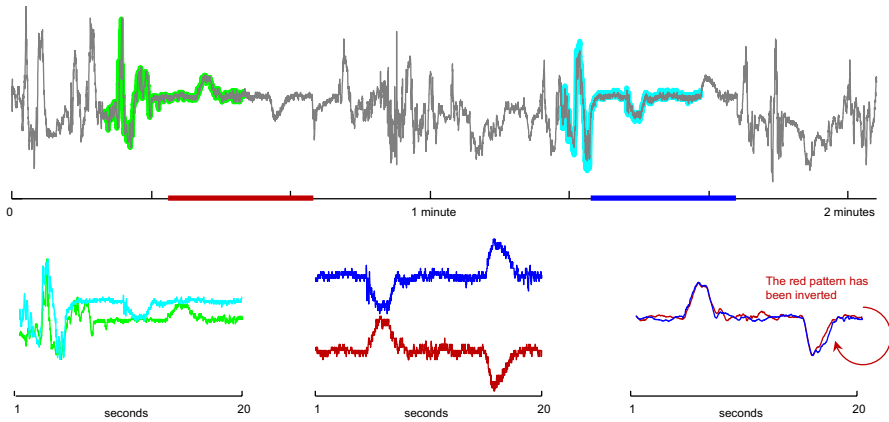
Fig. 6 (Top) Approximately 2 min from a dataset from a hip-worn accelerometer of quotidian activity. (Bottom left) The best motif of length 20-s is not well conserved, however, if we generalize the search to consider TSRC motifs (bottom center) we find a highly conserved pattern. To better see how well conserved it is, in (bottom right) we show the patterns with one element inverted, and both patterns smoothed. However, we note that we discovered this pattern in the original noisy space

For example, El Nino Southern Oscillation (ENSO) is a phenomenon that is characterized by intermittent negative correlations between the surface temperatures observed in the Central and Eastern Ocean (Kao and Yu 2009). However, there are much more quotidian examples. Consider the 2-min snippet of time series shown in Fig. 6. It shows the y-axis from a hip-worn accelerometer from the USC-HAD Database (Zhang and Sawchuk 2012). As shown in Fig. 6 bottom, left, the best motif of length 20-s is not well conserved, and almost looks like two random subsequences. This is unsurprising, apart from dance or athletic performances, we would not expect human behavior to faithfully repeat over such an extended time scale. However, we also searched for the best TSRC pattern of the same length, and as shown in Fig. 6 bottom center and bottom right it is stunningly well conserved.

What is the mechanism that produced this pattern? At about 22 s into the recording, the user stepped into an elevator. The first bump is the "jolt" of the elevator ascending, followed by the "dip-and-recover" as the elevator decelerated the desired floor. After about 1 min, the user took a return trip, descending the same number of floors.

The reader will readily appreciate that discovering TSRCs with the matrix profile is trivial, we simply used:

```
T2 = T*(-1);  % returns T flipped upside down
[JMP, JMPindex] = computeMatrixProfileJoin(T,T2,m);
```

Note that in this case, the discovered TSRC *also* happens to be a Semordnilap. However, this need not be the case in general.
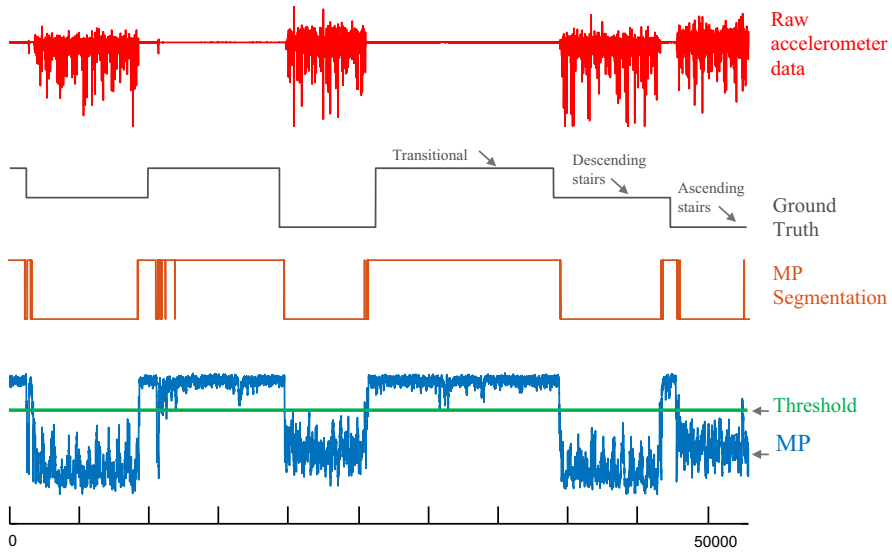
Fig. 7 (Top to bottom) A snippet of accelerometer data from Pamap Dataset-Subject 1, shoe-Acc *X*-axis, with its ground truth segmentation, into ascending stairs, descending stairs and transitional activities. The MP segmentation we predicted largely agrees, and was computed simply by thresholding the Matrix Profile. After casting the ground truth segmentation in a Boolean vector of {Transitional | other} we find out predicted segmentation agrees with it 93% of the time

3.4 Segmenting repetitive exercises

In recent years, there have been dozens of papers published on the task of segmenting repetitive exercises—such as weight training and calisthenics—via body worn sensors. See Morris et al. (2014) and the references therein and thereof. As Morris et al. (2014) forcefully argues, this problem is more difficult than it may seem at first glance. Many of the proposed methods use Hidden Markov Models, a powerful technique, but one that typically requires a lot of training data and careful parameter tuning. While we do not claim to be able to reproduce all the features of systems such as RecoFit (Morris et al. 2014), we note that at least in some cases, the Matrix Profile and a single line of extra code can segment repetitive exercises with high accuracy. Consider the following two lines of code.

```
[MP, MPindex] = computeMatrixProfile(T,m);

regions_of_repetition = MP < 2/3 * (min(MP)+max(MP));
```

We tested this code snippet on the Pamap Dataset (Reiss and Stricker 2012), a dataset frequently used by the relevant community. Figure 7 shows the result.

Why does this simple idea work so well? Note that activities such as ascending stairs and descending stairs correspond to very well-conserved, periodic movements

of the person, so such data would have a low matrix profile value. In contrast, the transitional activities are more at random, generating very noisy patterns with high matrix profile values. Therefore, in this dataset, a single threshold is enough for us to segment the activities.

3.5 Robust distance functions

Distance functions are at the heart of much of data mining, especially *time series* data mining (Batista et al. 2014). We can characterize distance functions by the invariances they achieve. For example (here we illustrate with *text*, the discrete analogue of time series):

- Euclidian distance is invariant to noisy data, and able to discover the similarity between `cat` and `rat`.
- Dynamic Time Warping is invariant to local misalignments in the data and differing data lengths, and able to discover the similarity between `concat` and `cooncat`.
- Cross Correlation is invariant to phase alignment, and can discover the similarity between `cathouse` and `housecat`.
- Longest Common Subsequence is invariant to minor insertions/deletion in the data and able to discover the similarity between `genome` and `gene`.

While there are many such distance measures to handle various distortions in *short* time series, *long* time series provide greater challenges. Consider the following phrases:

```
A = we can sequence the genome of the cat
B = the cats genome was sequenced in 2014
C = xe hes jlvoeqee kjsw eaqwe oqawe acea
```

Here the hamming distance (the discrete analogue of Euclidean Distance) between A and B is 31, but the distance between A and C is only 26. This is an unintuitive result, given that we immediately see the common structure in A and B. What we want is a distance measure that can reward A and B for sharing many subsequences, even if they are out of order. This issue also occurs for time series. To see this, we consider pairs of 10-s snippets extracted from four individuals experiencing cardiac issues. As shown in Fig. 8 left, we clustered them using a Euclidean distance average-linkage hierarchical clustering.

Here the disappointing results of Euclidean distance could be mitigated by very careful beat extraction and alignment. However, we want to be able to use distance functions with minimum human effort and knowledge. There are some distance functions that can achieve the required invariances. Their names, bag-of-patterns (Lin et al. 2012), bag-of-words (Wang et al. 2013), and so on suggest both their source of inspiration and their approach. While these methods may produce better

Fig. 8 (Left) Eight 10-s snippets of time series, from four individuals, clustered using Euclidean distance single-linkage hierarchical clustering. (Right) The same snippets clustered using a Matrix Profile based distance measure

results for our task at hand, they all have at least three parameters and require significant implementation effort. In the spirit of this work, can we reproduce at least *some* of their effort with the MP and a few lines of code? To answer this question, consider the following lines of code:

```
[JMP, dummy] = computeMatrixProfileJoin(A,B,m);
MSMD = min(JMP);
```

Using this MSMD distance measure, we produced the clustering shown in Fig. 8 right. Note that MSMD is symmetric: we can reverse the order of A and B in the pseudo code and obtain the same result. Assume S_A is a set of all subsequences extracted from time series A, and S_B is a set of all subsequences extracted from time series B, then MSMD is simply the minimum among all pairwise distances between subsequences from S_A and subsequences from S_B.

We can further test the utility of the MSMD distance measure, using classification. Almost all time series classification comparisons are based on the UCR archive (Batista et al. 2014; Ding et al. 2008). However most of the datasets in that archive are extracted from larger datasets with an extraction tool based on the Euclidian distance. Given that, it is hardly surprising that Euclidian distance (and DTW, which subsumes Euclidian distance as a special case) will be hard to beat (Ding et al. 2008). However, the newest release of the archive contains three related datasets that were processed in a different way. The source dataset is data from fifty-two pigs having three vital signs monitored, before and after an induced injury (Guillame-Bert and Dubrawski 2017). The data are vital signs measured at high frequency (250 Hz) using a bed-side hemodynamic monitoring system, much like a setup that one might expect to see in a modern ICU. The collected measurements are arterial

Table 1 A comparison of the holdout error rates of one-nearest neighbor with three distance measures. In each dataset, the default rate is 0.980, because each of the 52 pigs is equally likely

Dataset	MSMD (m)	Euclidian distance	DTW (w)
PigAirwayPressure	0.134 (425)	0.944	0.903 (1)
PigArtPressure	0.000 (140)	0.875	0.802 (1)
PigCVP	0.105 (200)	0.918	0.841 (11)

blood pressure, central venous pressure, and airway pressure. Critically for our purposes, the authors note "*Unlike in the* (pre-2018) *UCR data sets, the vital signs are not temporally aligned: the starting point of observation is effectively arbitrary*". We compared MSMD, Euclidian distance and DTW on the three pig datasets. We used the predefined train/test splits, learning MSMD's best value for *m*, and DTW's best value for *w* (the warping window width) with cross validation on just the training data. Table 1 summarizes the results.

The results show that while both Euclidian distance and DTW struggle to beat the default rate, the MSMD can achieve a very low error rate. It is possible that we could improve DTW by using endpoint invariance DTW, and we could improve Euclidian distance by doing circular shift Euclidian distance. However, these results strongly support our basic claim: you can get good results with the Matrix Profile and a handful of lines of code.

3.6 Meter-swapping detection

Electricity theft is a multi-billion-dollar problem worldwide (Sreenivasan 2016). There are dozens of ways to steal power, but some modern wireless meters offer a surprisingly easy method with little chance of detection (Kate and Rana 2015). Suppose customer **A** is a heavy consumer of electricity; perhaps he has several electric cars, or a machine shop, or a marijuana nursery in his garage. Further suppose that he notes that one of his neighbors, customer **B**, an elderly widow living alone, consumes very little power. It is possible for **A** to surreptitiously switch his meter with **B**, and thus only have to pay for her meager consumption, while she unwittingly gets lumbered with paying for his extravagant consumption. This crime is called *meter-swapping*, and has become increasingly prevalent as power companies have reduced meter reading staff in favor of wireless meter reading (Sreenivasan 2016).

It might be imagined that this would be easy for the power company to detect, as there would be a significant change in the average power consumed by two houses. However, as Fig. 9 top hints at, power consumption is often bursty anyway. For example, families take vacations, welcome a new baby, or have children return from college for a few weeks.

Our intuition to solve this problem is to note that while *volume* of consumption is not a good feature, some households may have a unique "shape" of the consumption over a day. Note that we do not expect *all* days to be conserved and unique, it is sufficient for our purposes that the household *occasionally* produces a well-conserved
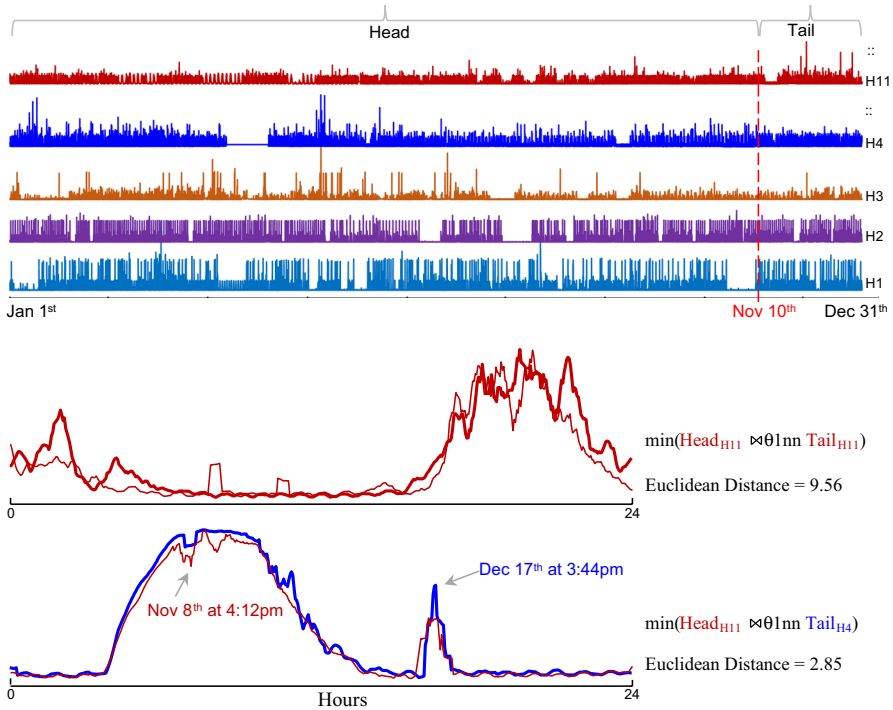
Fig. 9 (Top) Five time series from the set of 20 we consider for this demonstration, spanning from January 1st to December 23rd. A randomly chosen pair of time series had their "tails" (the region after November 10th) swapped to simulate a meter-swapping event. (Middle) If we join the head and tail of H11, the 1st motif pair has a mutual distance of 9.56, slightly lower than the mean of the motif distance for all 20 houses. (Bottom) If we join the head and tail pair from any of the 400 such combinations, the 1st motif pair from the join of $Head_{H11}$ and $Tail_{H4}$ produce the smallest mutual distance, of just 2.85; the motif patterns look strikingly similar

pattern, perhaps correspond to a low-power use on the Sabbath for an orthodox family, or (as in one of the authors' experience) an all-day obligation to wash and dry the soccer kits for the entire team once every 7 weeks.

We consider a dataset of household electrical power demand collected from twenty houses in the UK in 2013 (Murray et al. 2015). To simulate a meter-swapping event, we randomly chose two of these time series, and swapped their traces starting at November 10th. As we can see in Fig. 9 top this change is not readily visually obvious.

To find the swapped time series pair, we propose the following simple algorithm. We divide all the time series into two sections: the "Head," prior to November 10th and the "Tail," subsequent to November 10th. We join all possible combinations of Heads and Tails, and record the pair H_i, H_j that minimizes the following score:

$$\text{Swap-Score}(i, j) = \min(\text{Head}_{H_i} \bowtie \theta 1\text{nn Tail}_{H_j}) / (\min(\text{Head}_{H_i} \bowtie \theta 1\text{nn Tail}_{H_i}) + \text{epsilon})$$

In our simple experiment, this score was minimized by $i = $ H11 and $j = $ H4, which as it happens, *are* our swapped pair. As Fig. 9 bottom shows, the motif spanning these two apparently distinct traces time series is *suspiciously* similar, perhaps similar enough to warrant a visit by a meter reader/fraud prevention officer.

As before, the code to do this is trivial given the Matrix Profile:

```
for i=1:5
  [MP,MPindex] = computeMatrixProfileJoin(Head(i),Tail(i),m);
  minMP = min(MP) + eps % eps is Matlab's built-in epsilon
  for j=i+1:5   % Produce all pairs of Heads and Tails
    [JMP,JMPindex]=computeMatrixProfileJoin(Head(i),Tail(j),m);
    Score = min(JMP) / minMP ;
    <trivial code to maintain the minimum Score so far>
  end
end
```

Note that in our simple example we assumed we knew the date of the swap, removing that assumption would simply require expanding our search space.

3.7 Shapelet discovery

Time series shapelets are time series subsequences that best represent a class (Ye and Keogh 2009). The Matrix Profile can help us quickly identify good shapelet candidates. This idea was mentioned in passing in Yeh et al. (2016b) but was not fully developed and evaluated due to lack of space.

We demonstrate our approach with the GunPoint dataset. This dataset has two classes, Gun and NoGun (NoGun is also known as *Point*, hence the name GunPoint). As shown in Fig. 10, we construct time series T_A by concatenating all the instances of the Gun class, and construct time series T_B by concatenating all the instances of the NoGun class. We insert an *NaN* value in between every two concatenated instances to avoid introducing artificial patterns that are not present in the original time series. We then compute two matrix profiles, P_{BB} and P_{BA}. For simplicity, we use a subsequence length of 38, which is the length of the best shapelet reported for this dataset (Ye and Keogh 2009).

Intuitively, P_{BB} will be smaller than P_{BA} because we would expect subsequences within the same class to be more similar than those of different classes. The difference between P_{BA} and P_{BB} (we denote it as $P = P_{BA} - P_{BB}$), as shown in Fig. 10 bottom, generally agrees with this intuition.

We propose the peak values in P are indicators of good shapelet candidates, because they suggest patterns that are well conserved in their own class but are very different from their closest match in the other class. We pick the top-10
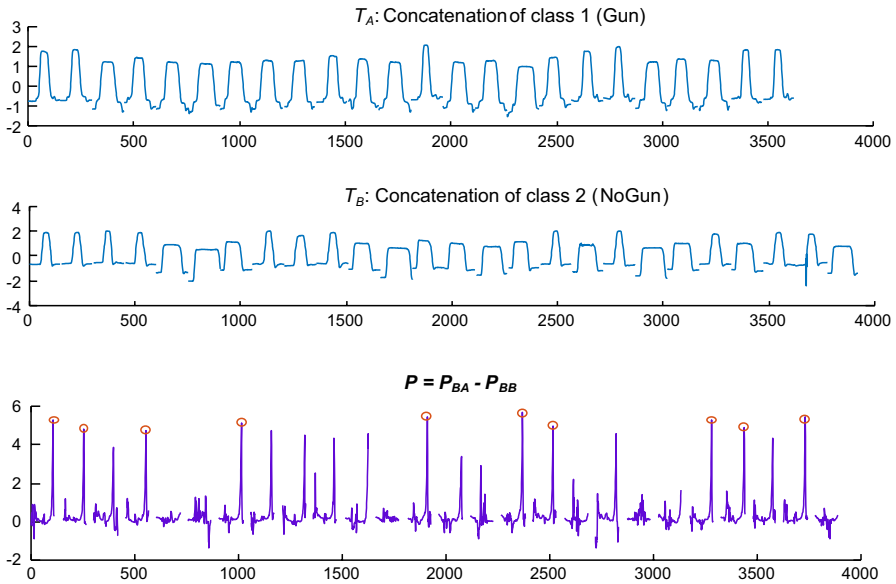
Fig. 10 (Top and middle) Two time series *A* and *B* formed by concatenating instances of each class of GunPoint dataset. (Bottom) The difference between P_{BA} and P_{BB}. The top-10 peak values (highlighted with red circles) are suggestive of good shapelet candidates (Color figure online)

candidates from T_B (analogously, we can find the top-10 candidates from T_A if we consider the difference between P_{AB} and P_{AA}). The code snippet is as follows.

```
[PBB, dummy] = computeMatrixProfileJoin(B, B, m);
[PBA, dummy] = computeMatrixProfileJoin(B, A, m);
MPdiff = PBA – PBB;
indicesOfTopShapelet  =  topTen(MPdiff);  % trivial  code  to
implement  topTen (extracting  the  top  10  peaks  from  the  matrix
profile) omitted
```

In Fig. 11 left, we can see that all the top-10 shapelets give very high classification accuracy on both the train and test data. Among them, we choose the one that renders the highest classification accuracy on the training set (the 6th shapelet) and show it in Fig. 11 right. This shapelet gives 93.33% accuracy on the test data, which is higher than the 91.33% accuracy of One-Nearest-Neighbor with DTW distance measure, with a bonus advantage of significantly less classification time. The shapelet learned reflects a distinct characteristic of the class that it represents (NoGun), as discussed by Ye and Keogh (2009): "*the NoGun class "has a "dip" where the actor put her hand down by her side, and inertia carries her hand a little too far and she is forced a correct it…a phenomenon known as 'overshoot'*". In contrast, in the opposite Gun class, the actor carries a gun. She
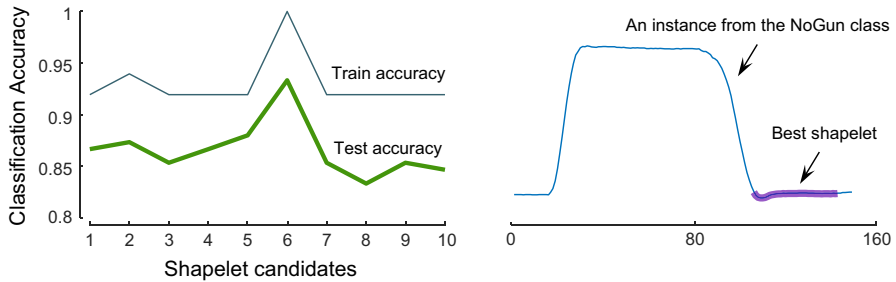
Fig. 11 (Left) Classification accuracy of the top-ten shapelet candidates. All the candidates render high classification accuracy on both train and test data. (Right) The best shapelet found in training. Classification with this shapelet on test data gives 93.33% accuracy, higher than the 91.33% accuracy of One-Nearest-Neighbor DTW. This 93.33% accuracy is also the best accuracy achieved with the classic shapelet search approach (Ye and Keogh 2009)

needs to put the gun back in the holster and then bring her hand to a complete rest position, generating a different pattern.

In hindsight, this shapelet also achieves the same classification accuracy on the test data as the original shapelet algorithm (Ye and Keogh 2009). However, in contrast to the classic shapelet algorithm, which exhaustively evaluates the classification power of every possible shapelet candidate in the dataset, the MP readily provides the top shapelet candidates for free.

3.8 Detecting and locating low frequency earthquakes

Low frequency earthquakes (LFEs), which recur episodically, could "*potentially contribute to seismic hazard forecasting by providing a new means to monitor slow slip at depth*" (Shelly et al. 2006). As such, detecting and locating LFEs are of great importance to the seismology community.

The waveforms of a recurring LFE recorded at the same seismic station are normally very similar to each other, as they reflect the unique signature of the wave reflecting and refracting through the local substrate. Thus, we can detect them by extracting the top motifs from the Matrix Profile of the continuous seismograph recording time series (e.g., Zhu et al. 2016). However, as indicated in Zhu et al. (2016), this can result in a lot of false positives since the sensor recording of a single seismic station often contains many repeating sensor artifacts or instrument noise. Though such false positives are easy to filter out by human eye (Zhu et al. 2016), this becomes untenable when the data is long enough to contain hundreds or thousands of false positive events. Figure 12 shows the matrix profile corresponding to a 24-h seismic recording of the FROB station near the central San Andreas fault at Parkfield, CA on Oct. 9th, 2007. The data is sampled at 20 Hz (1.728 million datapoints in total). The matrix profile contains hundreds of deep valleys, but only less than 10% of them are corresponding to true LFEs.

Is there a way to automatically filter out all the undesirable events (i.e., false positives)? Note that sensor artifacts or instrument noise are local (i.e., they will only be
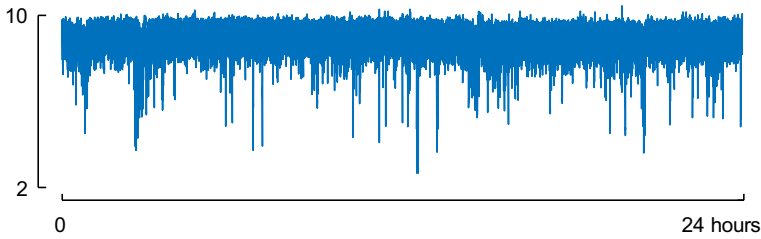
Fig. 12 The matrix profile of the FROB station on Oct 9th, 2007 contains a lot of deep valleys, a vast majority of which are false positives
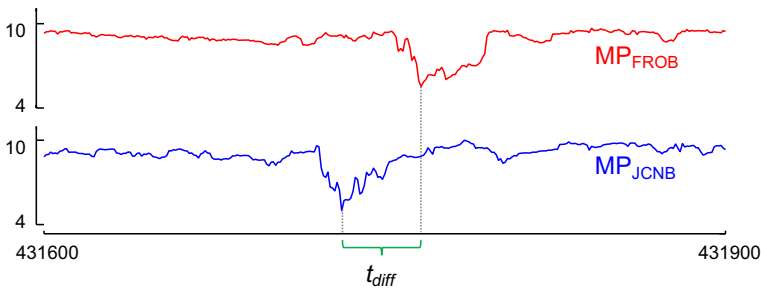

Fig. 13 (Top) A 15-s snippet of the matrix profile shown Fig. 12 at around 3 am. (Bottom) The same snippet of the matrix profile corresponding to the seismic recording of the nearby station JCNB. Both snippets contain a deep valley, but they are a little bit misaligned as the two stations receive the earthquake signal at slightly different times

detected by a single seismic station), while recurring LFEs can be detected by multiple stations at similar times. Correspondingly, we would expect the matrix profiles of multiple stations to show low values at the time when an LFE occurs. In contrast, when a false positive event occurs, only *one* of the matrix profiles would show low values and the others will show high values. This renders a simple solution to our problem: all we need to do is get the element-wise *maximum* of the matrix profiles corresponding to multiple nearby stations.

In Fig. 13 top we zoom in a 15-s snippet of the matrix profile shown in Fig. 12 at around 3am when an LFE occurs, and compare it with the same snippet taken from the matrix profile of a nearby seismic station JCNB (shown in Fig. 13 bottom). As expected, both snippets contain a valley.

However, note that the two valleys are slightly misaligned. This is because the source of the LFE locates slightly closer to the JCNB station than to the FROB station, and earthquakes travel at a finite speed. Thus, if we simply take the element-wise maximum of the two matrix profiles, the valley will become shallow. Fortunately, this misalignment (denoted as t_{diff} in Fig. 13 bottom) has physical limits: the two stations are about 10 km away, and the velocity of seismic waves near the surface of the earth is around 3–4 km/s, so t_{diff} cannot be more than 5 s (i.e., 100 data points). As such, we slightly adjust our "element-wise maximum" strategy to the following: we match the ith element of MP_{FROB} ($1 \leq i \leq |MP_{FROB}|$) to the minimum
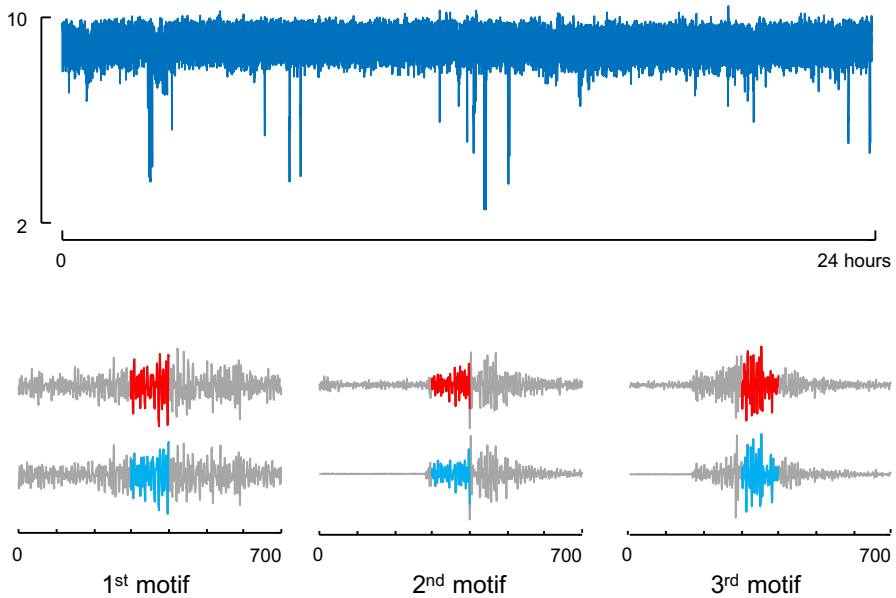
Fig. 14 (Top) The deep valleys in the resulting matrix profile all correspond to true events (compare to Fig. 12). (Bottom) The top 3 motifs extracted from the resulting matrix profile

element within the range $[\max(i-100, 1), \min(i+100, |\text{MP}_{\text{JCNB}}|)]$ of MP_{JCNB}, then take their maximum. The pseudo-code is as follows.

```
[MPfrob,dummy]=computeMatrixProfile(DATAfrob,m);  %FROB station
[MPjcnb,dummy]=computeMatrixProfile(DATAjcnb,m);  %JCNB station
Lfrob = length(MPfrob), Ljcnb = length(MPjcnb);
for i = 1 : Lfrob
    [minVal,minIdx]=min(MPjcnb(max(i-100,1):min(i+100,Ljcnb)));
    MPfrob(i) = max(MPfrob(i),minVal), Index(i) = minIdx;
end
```

Figure 14 top shows the resulting matrix profile `MPfrob`, which is much "cleaner" than the one shown in Fig. 12. We presented the top 10 motifs extracted from this matrix profile to a seismologist (Shakibay-Senobari 2018) (the top 3 are shown in Fig. 14 bottom), and he verified that they are all true LFEs.

Besides *detecting* true LFEs, note that our simple strategy also provides extra implications for *locating* the LFE*s*. The time difference t_{diff} shown in Fig. 13 can be found from the `Index` vector in our pseudocode, and if we know such time difference between 3 pairs of nearby seismic stations in the area, the exact location of the

source of the LFE can be calculated. We reserve detailed analysis and further demonstration of such considerations for future work.

3.9 Automatically clustering time series motifs

Building on our previous example we consider applications of the Matrix Profile to clustering of seismic data. Seismic waveform clustering has been applied to earthquake relocation (Trugman and Shearer 2017; Waldhauser and Ellsworth 2000; Richards-Dinger and Shearer 2000), repeating earthquake source identification (Geller and Mueller 1980; Nadeau et al. 1995; Vidale et al. 1994; Nadeau and McEvilly 1999; Beeler et al. 2001; Shelly et al. 2006; Wisely et al. 2008) and volcano monitoring (Sherburn et al. 1998; Lahr et al. 1994; Bardainne et al. 2006), helping to improve earthquake and volcanic hazard assessments. The seismology community has adopted various methods to cluster the seismic waveforms (time series subsequences corresponding to a seismic event) (Bardainne et al. 2006; Trugman and Shearer 2017). However, these methods take discrete, phase-aligned seismic waveforms of the same length as their input; extracting such waveforms from a long continuous seismic recording requires a lot of human effort. Here we introduce a simple method based on the Matrix Profile and ten lines of code, that can automatically discover earthquake pattern clusters from the continuous seismic recording.

To allow verification of the correctness of our result, we constructed a seismic time series by embedding twelve earthquake patterns into a 1000-s-long snippet of seismic background noise, as shown in Fig. 15a. The 12 embedded patterns are generated by four different earthquake sources (patterns of the same source are marked with the same color). The patterns corresponding to the same source normally look very similar to each other, while those corresponding to different sources are dissimilar. Our goal is to automatically discover the four natural clusters within the time series.

Before introducing our proposed solution, we would like to first dismiss some apparent solutions. Given the problem setting, the reader might consider finding the top-k motifs (Mueen et al. 2009) here. Note that the top-k motifs normally refer to the top-k most similar *pairs* of subsequences in the time series. However, from Fig. 15a we can see that a natural motif cluster can contain more than two occurrences of similar subsequences (e.g., the three red patterns are mutually similar); the classic top-k motif definition would separate them into different motif clusters, which is undesirable. The reader might also consider finding the *range* motifs (Mueen et al. 2009) instead of top-k motifs. However, discovering range motifs requires setting a threshold parameter r: the maximum distance between any two subsequences in a motif cluster must not be larger than $2r$. We argue that such threshold is very difficult to set and needs very careful tuning. For example, if two subsequences have a Euclidean distance of three, are they similar enough to be considered as a motif? The answer is not that obvious even for a domain expert who knows the data well.

Our solution can automatically find the natural number of motif clusters in the data (i.e., we do not need to specify how many clusters we would like to find), and requires only the setting of a much less critical parameter. The code is as follows:
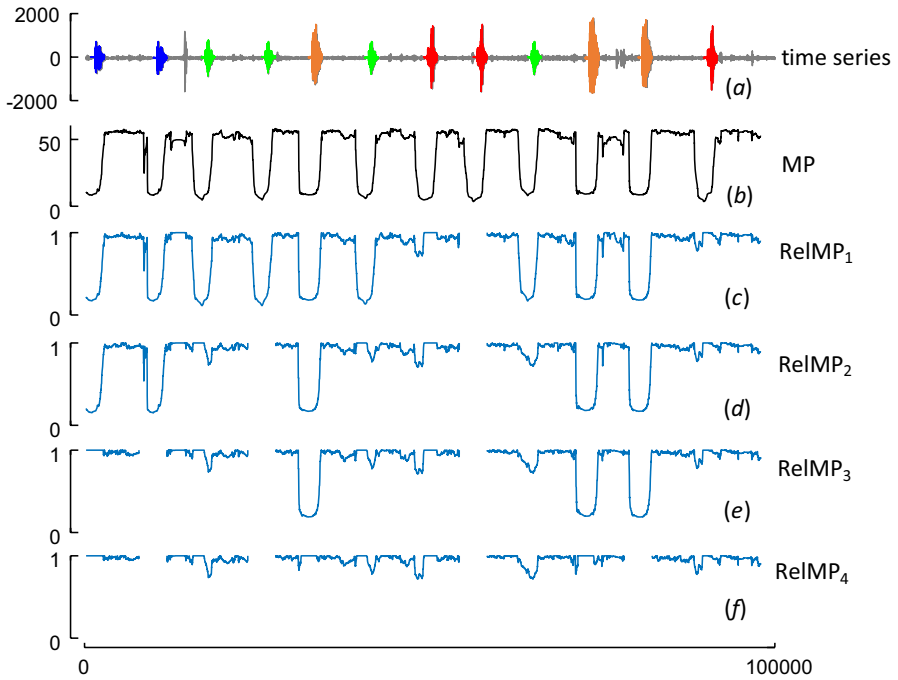
Fig. 15 (a) A seismic time series with 12 earthquake patterns. These earthquakes are generated by four different sources. Patterns corresponding to the same source are marked in the same color. (b) The matrix profile of the seismic time series. (c) The relative matrix profile after the 1st motif pattern is removed. The deep valleys corresponding to the three red patterns disappeared. (d) The relative matrix profile after the 2nd motif pattern is removed. The deep valleys corresponding to the four green patterns disappeared. (e) The relative matrix profile after the 3rd motif pattern is removed. The deep valleys corresponding to the two blue patterns disappeared. (f) The relative matrix profile after the 4th motif pattern is removed. The deep valleys corresponding to the three orange patterns disappeared (Color figure online)
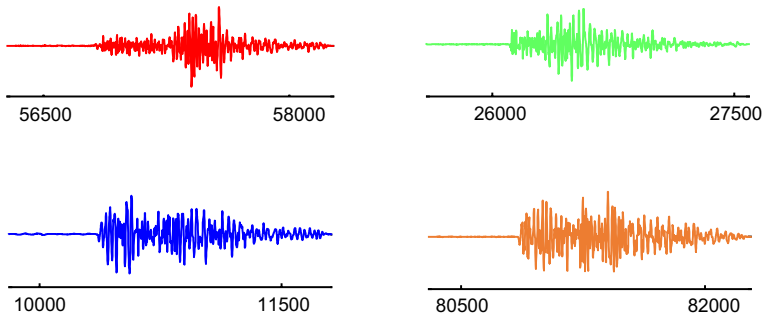
Fig. 16 (Top left) The 1st motif pattern discovered, corresponding to the minimum point of the matrix profile MP in Fig. 15b (top right). The 2nd motif pattern discovered, corresponding to the minimum point of the relative matrix profile RelMP$_1$ in Fig. 15c (bottom left). The 3rd motif pattern discovered, corresponding to the minimum point of the relative matrix profile RelMP$_2$ in Fig. 15d (bottom right) The 4th motif pattern discovered, corresponding to the minimum point of the relative matrix profile RelMP$_3$ in Fig. 15e

```
[MP, dummy] = computeMatrixProfile(T, m);
RelMP = MP, i = 1, DissMP = inf(1, length(MP));
while i == 1 || min(RelMP) < 0.2
    [minVal(i), minIdx(i)] = min(RelMP);
    DissmissRange = T(minIdx-m+1 : minIdx+2*m-2);
    [JMP, dummy] = computeMatrixProfileJoin(T,DissmissRange,m);
    DissMP = min(DissMP,JMP); %dismiss all motifs discovered so far
    RelMP = MP ./ DissMP;
    i = i + 1;
end
```

We first compute the matrix profile `MP` corresponding to the input time series `T`, as shown in Fig. 15b. We can see deep valleys in the vicinity of all the embedded earthquake patterns, as they all have close matches from the same source. We use the following iterative process to find the motif clusters one by one:

1. We find the minimum value in the current relative matrix profile `RelMP` (in the first iteration, we set `RelMP = MP`). This corresponds to a motif pattern (Fig. 16 shows the motif pattern discovered at each iteration).
2. We wish to avoid finding the same motif pattern in the next iteration. As such, we specify a `DissmissRange` which is a section of time series `T` that includes the current discovered motif pattern and its trivial matches, then compute the AB-join matrix profile `JMP` between the original time series `T` and `DissmissRange`.

JMP measures how similar each subsequence is to the *current* discovered motif pattern.

3. We use a vector DissMP to store the distance between every subsequence and its closest match among *all* the motif patterns discovered so far. DissMP is initialized as infinity, and once we have computed JMP, we update DissMP with the element-wise minimum of DissMP and JMP.

4. We evaluate a "relative" matrix profile RelMP by dividing the original matrix profile MP with DissMP. Our intuition is that, if a subsequence has a very close nearest neighbor, but is very different from any of the discovered motifs (and their trivial matches), then its RelMP value should be low. Note that the values in RelMP are always between 0 and 1.

5. If min(RelMP) < 0.2, go to step 1 and start the next iteration. Otherwise terminate the process.

From Fig. 15b–f, we can see how RelMP changes through this iterative process (we use RelMP_i to denote the status of RelMP at the end of the *i*th iteration). After each iteration, several deep valleys corresponding to the earthquake patterns in the same color disappeared from RelMP. The process terminates after the 4th iteration, when there are no more valleys apparent in RelMP.

The reader might wonder how we define "apparent valleys" here. We set a termination threshold as min(RelMP) = 1/5. Recall that RelMP(j) measures the relative ratio between MP(j), the distance from the *j*th subsequence to its nearest neighbor and DissMP(j), the distance from the *j*th subsequence to its closest match among all the discovered motif patterns. If the *j*th subsequence belongs to a new cluster, then it should be much more similar to its nearest neighbor than any of the discovered patterns. As such, we require that MP(j) cannot be more than 1/5 of DissMP(j).

From Fig. 16, we can see that the discovered motifs at different iterations correspond to different earthquake sources (different colors), and the process terminates right after we have discovered all the four embedded earthquake clusters.

3.10 Quantifying Parkinson disease

Parkinson Disease (PD) is a neuro-degenerative disease which affects gait and mobility. To assess the severity of the disease, clinicians use the Hoehn and Yahr scale (Afsar et al. 2018). The original scale published in 1967 (Hoehn and Yahr 1967) ranges from 1 to 5, with the scores 1.5 and 2.5 added in a later revision to allow doctors to describe the progression of the disease.

In a recent paper, the authors propose exploiting the "recurrence" of gait time series as a method to automatically score patients on the Hoehn and Yahr scale (Afsar et al. 2018). They use a mathematically sophisticated definition of recurrence based on an embedding in a phase space, showing that various heuristic complexity measures of the recurrence quantification analysis correlate to the Hoehn and Yahr scale.
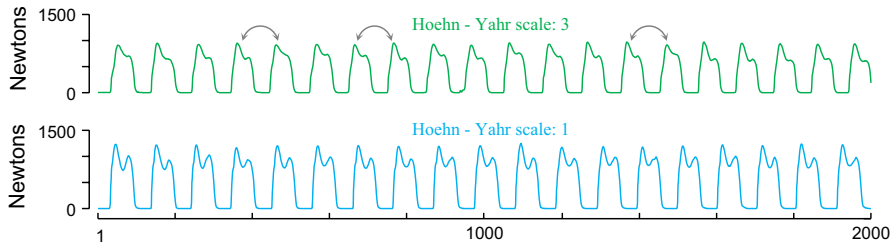
Fig. 17 A comparison of gait force profiles from two individuals walking for 20 s. One individual (top) was assessed by clinicians as being '3' on the Hoehn and Yahr scale. His gait cycles are not repeated perfectly, we have highlighted some of the most least conserved adjacent cycles. In contrast, another individual (bottom) who was assessed as '1' on the Hoehn and Yahr scale has a more conserved gait

The phase "recurrence" in the title of this paper caught our attention. Time series motifs are simple *recurring* subsequences. It is natural to ask if the Matrix Profile could be used for this task. Our intuition here is simple. Imagine a person could walk with a near perfectly repeated gait cycle. If we computed the matrix profile of their gait telemetry, we would expect the matrix profile values to be very small, as every subsequence would have a near perfect match somewhere. In contrast, if a person has an irregularity to their gait (caused by a tremor, a hesitation, or stumble), we would expect that these movements will add unique elements to each gait. As such, these unique gaits cycle will not find such close matches among their neighbors and therefore the matrix profile will be higher. In Fig. 17 we find some evidence to support the idea that people with more advanced PD have less well conserved gaits, at least on two randomly selected individuals.

To see if this observation is more generally true, we experimented with the Parkinson Disease (PD) dataset provided by Hausdorff group (Hausdorff et al. 1995), which is publicly available in "PhysioBank Database" (Goldberger et al. 2000). The data consists of gait force profiles of 93 patients with idiopathic PD (disease severity levels 2, 2.5 and 3 in terms of Hoehn–Yahr scale) and 73 healthy control individuals (who we would expect to score at level 1). The data consists of vertical ground reaction force of subjects when walking normally at their own pace. The ground reaction force is the force exerted by the ground on an object in contact with it, in this case, the object is the foot.

We propose using the median of MP of sensor data as a proxy for the severity level of PD. We use the median rather than the maximum or sum, as the latter two functions would be brittle to a single unusual step. By visual inspection it appears that, for all participants, the 20th step is vastly different for the rest, presumably as the patient reached the end of the apparatus and turned around.

We can compute the score for each patient with just:

Fig. 18 The median of the Matrix Profile versus the Hoehn–Yahr scale (red horizontal bar) plotted within classic box and whisker plots. Note that the median does increase with the severalty of the Hoehn–Yahr scale (Color figure online)
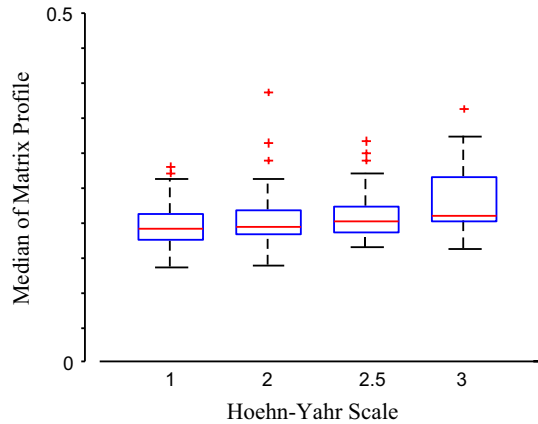

```
for i=1:size(1,patients)
  [MP,MPindex] = computeMatrixProfile(patients(i),100);
  HoehnYahrProxy = median(MP);
end
```

In Fig. 18 we show how well this proxy score models the Hoehn–Yahr scale.

It is important for us to disclaim that we are not making any medical claims for this experiment (we do not have such expertise), and we have not performed the type of statistical test that would pass muster in medical journal. Our point here, as always, is simply that the Matrix Profile and a few lines of code allow you to quickly test ideas that may be fruitful.

3.11 Scalability

Because the time taken for the Matrix Profile depends only on n, and not on the motif length m or the structure of the data, we can summarize the time complexly for *all* experiments with a single table as shown in Table 2. This is another very useful property of the Matrix Profile, which stands in contrast to almost all other methods. For example, *Quick-Motif* may be able to process a million datapoints on smooth data in about 4 min on a standard desktop (Li et al. 2015). But for noisier data, the time required could balloon by a factor of ten or more (Zhu et al. 2016).

The three computational approaches considered were: a standard desktop, a 72-core c5.18xlarge spot instance (Intel Skylake architecture), and an Amazon Web Service p3.2xlarge (1 Tesla V100) which cost about 3.06 USD/hour at the time of writing.

Note that the time taken for the desktop version does get prohibitive for large datasets. However, note that the if the data discussed in Sect. 3.1 was sampled at

Table 2 Time taken to compute a Matrix Profile for datasets ranging from 2^{18} to 2^{23} using three computational paradigms

Input size	Instance type			
	Experiments of that size	Desktop CPU seconds	c5.18xlarge (72 cores) 3.06 USD/h seconds	p3.2xlarge (1 Tesla V100) 3.06 USD/h seconds
2^{18}	3.2, 3.3, 3.4, 3.7, 3.9, 3.10	6.4	7	0.28
2^{19}	3.5	25.3	14	0.68
2^{20}	3.6	99.9	32	2.00
2^{21}	3.8	397.8	76	7.00
2^{22}		1584.8	252	25.80
2^{23}	3.1	6333.3	933	96.80

Note that for small datasets a standard desktop can beat HPC due to setup costs, but that advantage disappears as we see larger datasets

1 Hz, then the 6,106,456 datapoints would represent about 70 days. Thus, even if we use a standard desktop, we can compute the Matrix Profile about 1000 times faster than real-time for this problem. Moreover, recall that this is for the fully converged Matrix Profile. As Zhu et al. (2018) shows, we can typically closely approximate in the Matrix Profile in about 1/100th of the time to complete convergence.

4 Conclusion

We have presented ten time series data mining case studies in which interesting and actionable results can be obtained given just a handful of lines of code. Moreover, these results can be obtained essentially instantaneously, given our assumption that the computation of the Matrix Profile is free. That last assumption needs a little qualification. The existing Matrix Profile algorithms, STAMP (Yeh et al. 2016b), and STOMP (Zhu et al. 2016) are effectively instantaneously for many end users, who have only tens of thousands of data points. For example, the Parkinson Disease, music processing, and classification (shapelet) examples all have this property. For users with say one-hundred thousand to one million datapoints, they may need to wait minutes for their results. Our meter-swapping example is of this scale. Note, however, that the minutes of computation time are dwarfed by the full year of time it took to collect the data. For users with datasets in the many millions, computation time becomes more of an issue, but even here there is hope on the horizon. In a recently published paper we introduced a novel algorithm called SCRIMP++ (Zhu et al. 2018) that can approximate the Matrix Profile even faster than STAMP, allowing a user with say a million datapoints to obtain a high quality approximate Matrix Profile in "interactive" time (a handful of seconds), and in an upcoming work we will show that a GPU cluster optimized algorithm called SCAMP can scale up to

billion length time series. Moreover, we suspect that others in the community will find ways to accelerate the Matrix Profile that did not occur to us.

References

Afsar O, Tirnakli U, Marwan N (2018) Recurrence Quantification Analysis at work: quasi-periodicity based interpretation of gait force profiles for patients with Parkinson disease. Sci Rep 8(1):9102

Bardainne T, Gaillot P, Dubos-Sallée N, Blanco J, Sénéchal G (2006) Characterization of seismic waveforms and classification of seismic events using chirplet atomic decomposition. Example from the Lacq gas field (Western Pyrenees, France). Geophys J Int 166(2):699–718

Batista GEAPA, Keogh EJ, Tataw OM, De Souza VMA (2014) CID: an efficient complexity-invariant distance for time seriem. Data Min Knowl Discov 28(3):634–669

Bayardo RJ, Ma Y, Srikant R (2007) Scaling up all pairs similarity search. In: Proceedings of the 16th international conference on World Wide Web (WWW), pp 131–140

Beeler NM, Lockner DL, Hickman SH (2001) A simple stick-slip and creep-slip model for repeating earthquakes and its implication for microearthquakes at Parkfield. Bull Seismol Soc Am 91(6):1797–1804

Bonds ME (1998) Haydn's' Cours complet de la composition' and the Sturm und Drang. Haydn studies, pp 152–176

Chandola V, Cheboli D, Kumar V (2009) Detecting anomalies in a time series database. UMN TR09-004

Chen Y, Keogh E, Hu B, Begum N, Bagnall A, Mueen A, Batista G (2015) The UCR time series classification archive. http://www.cs.ucr.edu/~eamonn/time_series_data/

Ding H, Trajcevski G, Scheuermann P, Wang X, Keogh EJ (2008) Querying and mining of time series data: experimental comparison of representations and distance measures. Proc VLDB Endow (VLDB) 1(2):1542–1552

Geller RJ, Mueller CS (1980) Four similar earthquakes in central California. Geophys Res Lett 7(10):821–824

Gharghabi S, Ding Y, Yeh CCM, Kamgar K, Ulanova L, Keogh E (2017) Matrix profile VIII: domain agnostic online semantic segmentation at superhuman performance levels. In: Proceedings of the 2017 IEEE international conference on data mining (ICDM), pp 117–126

Goldberger AL, Amaral LA, Glass L, Hausdorff JM, Ivanov PC, Mark RG, Mietus JE, Moody GB, Peng CK, Stanley HE (2000) PhysioBank, PhysioToolkit, and PhysioNet: components of a new research resource for complex physiologic signals. Circulation 101(23):e215–e220

Guillame-Bert M, Dubrawski A (2017) Classification of time sequences using graphs of temporal constraints. J Mach Learn Res 18(1):4370–4403

Gupta S, Reynolds MS, Patel SN (2010) ElectriSense: single-point sensing using EMI for electrical event detection and classification in the home. In: Proceedings of the 12th ACM international conference on ubiquitous computing, pp 139–148

Hausdorff JM, Ladin Z, Wei JY (1995) Footswitch system for measurement of the temporal parameters of gait. J Biomech 28(3):347–351

Hoehn MM, Yahr MD (1967) Parkinsonism: onset, progression and mortality. Neurology 17(5):427–442

Kao HY, Yu JY (2009) Contrasting eastern-Pacific and central-Pacific types of ENSO. J Clim 22(3):615–632

Kate PG, Rana JR (2015) ZIGBEE based monitoring theft detection and automatic electricity meter reading. In: Proceedings of the 2015 International conference on energy systems and applications, pp 258–262

Kurpiewski MR, Engler LE, Wozniak LA, Kobylanska A, Koziolkiewicz M, Stec WJ, Jen-Jacobson L (2004) Mechanisms of coupling between DNA recognition specificity and catalysis in EcoRI endonuclease. Structure 12(10):1775–1788

Lahr JC, Chouet BA, Stephens CD, Powers JA, Page RA (1994) Earthquake classification, location, and error analysis in a volcanic environment: implications for the magmatic system of the 1989–1990 eruptions at Redoubt Volcano, Alaska. J Volcanol Geotherm Res 62:137–152

LG Dishwasher Owners Manual (2017) http://www.lg.com/us/support/products/documents/Owners%20 Manual.pdf. Accessed 2 Dec 2017

Li Y, Yiu ML, Gong Z (2015) Quick-motif: An efficient and scalable framework for exact motif discovery. In: Proceedings of the 2015 IEEE 31st international conference on data engineering (ICDE), pp 579–590

Lin J, Khade R, Li Y (2012) Rotation-invariant similarity in time series using bag-of-patterns representation. J Intell Inf Syst 39(2):287–315

Morris D, Saponas TS, Guillory A, Kelner I (2014) RecoFit: using a wearable sensor to find, recognize, and count repetitive exercises. In: Proceedings of the 2014 SIGCHI conference on human factors in computer systems, pp 3225–3234

Mueen A, Keogh E, Zhu Q, Cash S, Westover B (2009) Exact discovery of time series motif. In: Proceedings of the 2009 SIAM international conference on data mining (SDM), pp 473–484

Murray D, Liao J, Stankovic L, Stankovic V, Hauxwell-Baldwin R, Wilson C, Coleman M, Kane T, Firth S (2015) A data management platform for personalised real-time energy feedback. In: Proceedings of the 8th international conference on energy efficiency in domestic appliances and lighting (EEDAL), pp 1–15

Music Performance (2017) Joseph Haydn's symphony no. 47 in G major, by the Tafelmusik Orchestra. www.youtube.com/watch?v=yeB_Ohpsm64. Accessed 2 Dec 2017

Nadeau RM, McEvilly TV (1999) Fault slip rates at depth from recurrence intervals of repeating microearthquakes. Science 285(5428):718–721

Nadeau RM, Foxall W, McEvilly TV (1995) Clustering and periodic recurrence of microearthquakes on the San Andreas Fault at Parkfield, California. Science 267(5197):503–507

Puder J (2000) Seventeen synonyms of Semordnilap. Word Ways 33(1), article 9

Reiss A, Stricker D (2012) Introducing a new benchmarked dataset for activity monitoring. In: Proceedings of the 16th international symposium on wearable computers (ISWC), pp 108–109

Richards-Dinger KB, Shearer PM (2000) Earthquake locations in southern California obtained using source-specific station terms. J Geophys Res Solid Earth 105(B5):10939–10960

Shakibay-Senobari N (2018) Personal correspondence. June 14, 2018

Shelly DR, Beroza GC, Ide S, Nakamula S (2006) Low-frequency earthquakes in Shikoku, Japan, and their relationship to episodic tremor and slip. Nature 442(7099):188–191

Sherburn S, Scott BJ, Nishi Y, Sugihara M (1998) Seismicity at White Island volcano, New Zealand: a revised classification and inferences about source mechanism. J Volcanol Geoth Res 83(3–4):287–312

Sreenivasan G (2016) Power theft. PHI Learning Pvt. Ltd, New Delhi

Supporting Webpage (2019) https://sites.google.com/site/matrixprofiletopten/

Tasmanian devil (2017) Wikipedia, the free encyclopedia. https://en.wikipedia.org/wiki/Tasmanian_devil

The UCR Matrix Profile Page (2017) www.cs.ucr.edu/~eamonn/MatrixProfile.html. Accessed 2 Dec 2017

Trugman DT, Shearer PM (2017) GrowClust: a hierarchical clustering algorithm for relative earthquake relocation, with application to the Spanish Springs and Sheldon, Nevada, earthquake sequences. Seismol Res Lett 88(2A):379–391

Vidale JE, Ellsworth WL, Cole A, Marone C (1994) Variations in rupture process with recurrence interval in a repeated small earthquake. Nature 368(6472):624–629

Waldhauser F, Ellsworth WL (2000) A double-difference earthquake location algorithm: method and application to the northern Hayward fault. Bull Seismol Soc Am 90(6):1353–1368

Wang J, Liu P, She MF, Nahavandi S, Kouzani A (2013) Bag-of-words representation for biomedical time series classification. Biomed Signal Process Control 8(6):634–644

Wisely BA, Schmidt DA, Weldon II RJ (2008) Compilation of surface creep on California faults and comparison of WGCEP 2007 deformation model to Pacific-North American plate motion (No. 2007-1437-P). Geological Survey (US)

Yankov D, Keogh E, Medina J, Chiu B, Zordan V (2007) Detecting time series motifs under uniform scaling. In: Proceedings of the 2007 ACM SIGKDD international conference on knowledge discovery and data mining, pp 844–853

Ye L, Keogh E (2009) Time series shapelets: a new primitive for data mining. In: Proceedings of the 2009 ACM SIGKDD international conference on knowledge discovery and data mining, pp 947–956

Yeh CCM, Herle HV, Keogh E (2016a) Matrix profile III: the matrix profile allows visualization of salient subsequences in massive time series. In: Proceedings of the 2016 IEEE international conference on data mining (ICDM), pp 579–588

Yeh CCM, Zhu Y, Ulanova L, Begum N, Ding Y, Dau HA, Silva DF, Mueen A, Keogh E (2016b) Matrix profile I: all pairs similarity joins for time series: a unifying view that includes motifs, discords and shapelets. In: Proceedings of the 2016 IEEE international conference on data mining (ICDM), pp 1317–1322

Yeh CCM, Kavantzas N, Keogh E (2017) Matrix profile IV: using weakly labeled time series to predict outcomes. Proc VLDB Endow (VLDB) 10(12):1802–1812

Yeh CCM, Zhu Y, Ulanova L, Begum N, Ding Y, Dau HA, Zimmerman Z, Silva DF, Mueen A, Keogh E (2018) Time series joins, motifs, discords and shapelets: a unifying view that exploits the matrix profile. Data Min Knowl Disc 32(1):83–123

Zhang M, Sawchuk A (2012) USC-HAD: a daily activity dataset for ubiquitous activity recognition using wearable sensors. In: Proceedings of the 2012 ACM conference on ubiquitous computing, pp 1036–1043

Zhu Y, Zimmerman Z, Senobari NS, Yeh CCM, Funning G, Mueen A, Brisk P, Keogh E (2016) Matrix profile II: exploiting a novel algorithm and GPUS to break the one hundred million barrier for time series motifs and joins. In: Proceedings of the 2016 IEEE international conference on data mining (ICDM), pp 739–748

Zhu Y, Imamura M, Nikovski D, Keogh E (2017) Matrix profile VII: time series chains: a new primitive for time series data mining. In: Proceedings of the 2017 IEEE international conference on data mining (ICDM), pp 695–704

Zhu Y, Yeh CCM, Zimmerman Z, Kamgar K, Keogh E (2018) Matrix profile XI: SCRIMP++: time series motif discovery at interactive speeds. In: Proceedings of the 2018 IEEE international conference on data mining (ICDM), pp 837–846